Liquid-crystal-mediated force between a cylindrical nanoparticle and substrate

David L. Cheung* and Michael P. Allen†
Department of Physics and Centre for Scientific Computing, University of Warwick, Coventry CV4 7AL, United Kingdom
(Received 23 April 2007; published 25 October 2007)

Using classical density functional theory, the structure of a molecular fluid around a cylindrical nanoparticle near a solid substrate is studied. The solvent-mediated force between the nanoparticle and the substrate is calculated in both the nematic and isotropic phases of the solvent. In the nematic phase, the force is short ranged and arises due to interaction between high-density regions near the substrate and nanoparticle. In the isotropic phase, the formation of a nematic bridge between the substrate and nanoparticle gives rise to an attractive force between them. The potential between the nanoparticle and substrate as a function of separation calculated numerically is compared to that calculated from the Derjaguin approximation. In the isotropic phase these are found to be in reasonable agreement at low separations, while the agreement is poorer in the nematic phase.

DOI: 10.1103/PhysRevE.76.041706 PACS number(s): 61.30.Cz, 61.20.Gy, 61.30.Jf, 61.30.Hn

I. INTRODUCTION

Dispersions of solid particles in liquid crystals (LCs) comprise an interesting class of novel materials [1,2]. In the nematic phase, formation of topological defects around solid particles leads to long-range interactions between them. Above the isotropic-nematic transition, attractive interactions between the particles arise due to halos of ordered fluid adsorbed on their surfaces. There are a wide range of applications of colloidal dispersions in LCs [3,4], with particular emphasis on dispersions of anisotropic particles such as clay platelets [5] and magnetic nanowires in LCs [6]. In many instances, the interactions between colloids and solid interfaces is of particular importance, examples including LC biosensors [7] and alignment of carbon nanotubes by LCs [8].

Solvent-mediated forces, such as the depletion interaction, play an important role in the interactions between colloidal particles and substrates. When the colloidal particles are dispersed in a nematic LC, elastic forces due to the distortion of the director act on the particle [9]. In the isotropic phase, capillary condensation between the particle and substrate occurs near the isotropic-nematic transition [10,11]. For colloidal particles significantly larger than the size of LC molecules, where variation in the solvent density may be neglected, phenomenological theories have been employed. When the size of the colloidal particles is in the range of nanometers this density variation is likely to become significant [12] so must be taken into account when studying such systems. It is also experimentally challenging to study particles of this size range.

In a recent paper [13], density functional theory (DFT) at the level of the Onsager second virial approximation [14] was used to study the structure of a liquid crystalline fluid around a single cylindrical nanoparticle. This was found to give results consistent with both molecular simulations and phenomenological theories, while being less computationally expensive than the former and while accounting for the spatial variation of the molecular density. Here, that work is extended to study such nanoparticles in the vicinity of solid substrates in both the nematic and isotropic phases of the solvent. Experimental [15,16] studies of similar systems have shown a rich phenomenology. Considering the interaction between a colloid and a substrate also offers insights into interactions between colloidal particles [17,18].

This paper is organized as follows. The theory and computational method used in this work are outlined in the next section. The results of this work are then presented, detailing the structure of fluid around nanoparticles in the vicinity of a planar substrate and the potential as a function of nanoparticle-substrate separation. The effect of nematic bridging between the nanoparticle and substrate is also discussed, and our numerical results are compared to analytic approximations.

II. THEORY

The liquid crystal solvent is modeled as a fluid of hard ellipsoids of aspect ratio $e=a/b=15$ (in the rest of this paper $b=1$ will be taken to be the unit of length). While a gross simplification, such hard body models show very similar behavior to real LC systems [19]. The grand potential of such a system may be written as [20]

$$\beta\Omega[\rho(\boldsymbol{r},\boldsymbol{u})] = \beta F_{\mathrm{id}}[\rho(\boldsymbol{r},\boldsymbol{u})] + \beta F_{\mathrm{ex}}[\rho(\boldsymbol{r},\boldsymbol{u})] + \beta \int d\boldsymbol{r}\, d\boldsymbol{u}[V_{\mathrm{ext}}(\boldsymbol{r},\boldsymbol{u}) - \mu]\rho(\boldsymbol{r},\boldsymbol{u}), \quad (1)$$

where $\rho(\boldsymbol{r},\boldsymbol{u})$ is the position- and orientation-dependent single-particle density, $V_{\mathrm{ext}}(\boldsymbol{r},\boldsymbol{u})$ is the external potential, μ is the chemical potential, and $\beta=1/k_BT$. $F_{\mathrm{id}}[\rho(\boldsymbol{r},\boldsymbol{u})]$ and $F_{\mathrm{ex}}[\rho(\boldsymbol{r},\boldsymbol{u})]$ are the ideal and excess free energies, respectively. $\boldsymbol{r}$ is the position vector and $\boldsymbol{u}$ is the orientation vector. The ideal free energy is given by

$$\beta F_{\mathrm{id}}[\rho(\boldsymbol{r},\boldsymbol{u})] = \int d\boldsymbol{r}\, d\boldsymbol{u}\ \rho(\boldsymbol{r},\boldsymbol{u})[\ln \rho(\boldsymbol{r},\boldsymbol{u}) - 1]. \quad (2)$$

The exact form of the excess free energy is generally unknown. Here we employ the Onsager approximation [14]

*david.cheung@warwick.ac.uk
†m.p.allen@warwick.ac.uk

$$\beta F_{\rm ex}[\rho(\boldsymbol{r},\boldsymbol{u})] = -\frac{1}{2}\int d\boldsymbol{r}_1 d\boldsymbol{r}_2 d\boldsymbol{u}_1 d\boldsymbol{u}_2 f(\boldsymbol{r}_{12},\boldsymbol{u}_1,\boldsymbol{u}_2) \times \rho(\boldsymbol{r}_1,\boldsymbol{u}_1)\rho(\boldsymbol{r}_2,\boldsymbol{u}_2), \quad (3)$$

where $\boldsymbol{r}_{12}=\boldsymbol{r}_1-\boldsymbol{r}_2$ and $f(\boldsymbol{r}_{12},\boldsymbol{u}_1,\boldsymbol{u}_2)=\exp[-\beta V(\boldsymbol{r}_{12},\boldsymbol{u}_1,\boldsymbol{u}_2)]-1$ is the Mayer function. $V(\boldsymbol{r}_{12},\boldsymbol{u}_1,\boldsymbol{u}_2)$ is the intermolecular potential, where $V=\infty$ ($f=-1$) when two molecules overlap and $V=0$ ($f=0$) otherwise. Although Eq. (3) is only exact for infinite elongations, previous studies [21] have shown that there is good agreement between Onsager theory and simulation for the elongation used in this study ($e=15$). In contrast, for shorter elongations, such as the $e=5$ ellipsoids used in previous work [13], the isotropic-nematic transition densities are greatly overestimated by Onsager theory. The external potential, representing a single cylindrical nanoparticle of radius R oriented along the y axis, is given by

$$V_{\rm ext}(\boldsymbol{r},\boldsymbol{u}) = V_{\rm ext}(\boldsymbol{s},\boldsymbol{u}) = \begin{cases} V_0[\tanh(b/w)], & s-R<-b, \\ \frac{1}{2}V_0\left[\tanh\left(\frac{R-s}{w}\right)+\tanh(b/w)\right], & |s-R|<b, \\ 0, & s-R>b, \end{cases} \quad (4)$$

where $\boldsymbol{s}=(x,z)$, $s=|\boldsymbol{s}|$, $V_0=50k_BT$, and $w=b/5$. This represents a sharply varying repulsive potential acting on the ellipsoid centers of mass; it excludes the molecules from the cylinder and gives rise to homeotropic (normal) anchoring at the surface. In comparison with the planar anchoring case, this gives rise to a more complex director configuration around an isolated particle [22]. Nanoparticles with radii $R=15b$ and $30b$ have been studied (one and two molecular length, respectively). The relative sizes of the solvent molecules and nanoparticle are similar to those of a typical LC [e.g., for 4–cyano–4'–n'pentylbiphenyl (5CB) $a\approx 1.8$ nm] and typical inorganic nanoparticles [4] or proteins and other biomolecules [23] (3–20 nm). The substrate is modeled as step function acting on the centers of mass of the ellipsoids, which again gives rise to homeotropic alignment.

Following previous work [13], the angularly dependent functions are expanded in a set of spherical harmonics:

$$\ln \rho(\boldsymbol{r},\boldsymbol{u}) = \sum_{\ell,m} \tilde{\rho}_{\ell m}(\boldsymbol{s}) Y_{\ell m}(\boldsymbol{u}), \quad (5a)$$

$$\rho(\boldsymbol{r},\boldsymbol{u}) = \sum_{\ell,m} \rho_{\ell m}(\boldsymbol{s}) Y^*_{\ell m}(\boldsymbol{u}), \quad (5b)$$

$$V_{\rm ext}(\boldsymbol{r},\boldsymbol{u}) = \sum_{\ell,m} V_{\ell m}(\boldsymbol{s}) Y_{\ell m}(\boldsymbol{u}), \quad (5c)$$

where translational invariance along y allows us to write the coefficients as functions of $\boldsymbol{s}$. Note the complex conjugate in the density expansion. The Mayer function is expanded as [24]

$$f(\boldsymbol{r}_{12},\boldsymbol{u}_1,\boldsymbol{u}_2) = \sum_{\ell_1,\ell_2,\ell} f_{\ell_1\ell_2\ell}(r_{12})\Phi_{\ell_1\ell_2\ell}(\hat{\boldsymbol{r}}_{12},\boldsymbol{u}_1,\boldsymbol{u}_2), \quad (6)$$

where $r_{12}=|\boldsymbol{r}_{12}|$, $\hat{\boldsymbol{r}}_{12}=\boldsymbol{r}_{12}/r_{12}$, and $\Phi_{\ell_1\ell_2\ell}$ is a rotational invariant [25]. Inserting these expressions into Eq. (1) and integrating over angles and the y direction gives the grand potential (per unit length along the y direction denoted as L)

$$\frac{\beta\Omega[\rho(\boldsymbol{r},\boldsymbol{u})]}{L} = \int d\boldsymbol{s}\sum_{\ell,m}\rho_{\ell m}(\boldsymbol{s})[\tilde{\rho}_{\ell m}(\boldsymbol{s}) - \sqrt{4\pi}(1+\beta\mu)\delta_{l0} + \beta V_{\ell m}(\boldsymbol{s})] + \int d\boldsymbol{s}_1 d\boldsymbol{s}_2 \sum_{\substack{\ell_1,m_1\\ \ell_2,m_2}} \mathcal{L}_{\ell_1 m_1 \ell_2 m_2}(\boldsymbol{s}_{12}) \times \rho_{\ell_1 m_1}(\boldsymbol{s}_1)\rho_{\ell_2 m_2}(\boldsymbol{s}_2). \quad (7)$$

The quantities $\mathcal{L}_{\ell_1 m_1 \ell_2 m_2}(\boldsymbol{s}_{12})$ come from integrating the Mayer function and are the spherical harmonic coefficients of the excluded length (in the y direction) of two molecules with a separation vector $\boldsymbol{s}_{12}=\boldsymbol{s}_1-\boldsymbol{s}_2$ in the xz plane, treated as a function of the molecular orientations. As the last term in Eq. (7) is a convolution, it is most conveniently evaluated in reciprocal space. If $\rho_{lm}(\boldsymbol{k})$ is the two-dimensional Fourier transform of $\rho_{lm}(\boldsymbol{s})$ then this term may be written

$$\sum_{\boldsymbol{k}}\sum_{\substack{\ell_1,m_1\\ \ell_2,m_2}} \mathcal{L}_{\ell_1 m_1 \ell_2 m_2}(\boldsymbol{k})\rho_{\ell_1 m_1}(\boldsymbol{k})\rho_{\ell_2 m_2}(\boldsymbol{k}), \quad (8)$$

where $\mathcal{L}_{\ell_1 m_1 \ell_2 m_2}(\boldsymbol{k})$ is the Fourier transform of $\mathcal{L}_{\ell_1 m_1 \ell_2 m_2}(\boldsymbol{s}_{12})$.

In order to find the equilibrium density, the functions are tabulated on a regular grid in the xz plane; the grid spacing is $\delta x=\delta z=0.5b$, the molecular length corresponding to 30 grid points. The grand potential is then minimized with respect to the $\tilde{\rho}_{\ell m}(\boldsymbol{s})$ coefficients at each grid point using the conjugate gradient method [26]. When required, the coefficients $\rho_{\ell m}(\boldsymbol{s})$ are calculated through Eqs. (5), with angular integrations performed using Lebedev quadrature [27,28].

Once the equilibrium density coefficients $\rho_{\ell m}(\boldsymbol{s})$ have been determined, the number density $\rho(\boldsymbol{s})$ and order tensor $Q_{\alpha\beta}(\boldsymbol{s})$ may be found from

$$\rho(\boldsymbol{s}) = \int d\boldsymbol{u}\ \rho(\boldsymbol{s},\boldsymbol{u}) = \sqrt{4\pi}\rho_{00}(\boldsymbol{s}), \quad (9)$$

$$Q_{\alpha\beta}(\boldsymbol{s}) = \frac{3}{2}\int d\boldsymbol{u}\ \rho(\boldsymbol{s},\boldsymbol{u})u_\alpha(\boldsymbol{s})u_\beta(\boldsymbol{s}) - \frac{1}{2}\delta_{\alpha\beta}, \quad \alpha,\beta = x,y,z. \quad (10)$$

The spatially varying order parameter $S(\boldsymbol{s})$ is given by the largest eigenvalue of $Q_{\alpha\beta}(\boldsymbol{s})$ and the director $\boldsymbol{n}(\boldsymbol{s})$ by the eigenvector associated with $S(\boldsymbol{s})$.

III. RESULTS

Shown in Figs. 1 and 2 are the density and order parameter maps for single nanoparticles in the nematic and isotropic phases. In both cases, the structure of the fluid around the cylinder is in accordance with previous work, both theoreti-

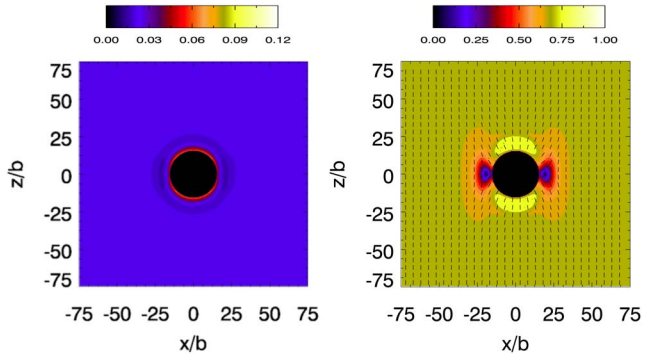

FIG. 1. (Color online) Density (left) and order parameter (right) maps for isolated cylinder in the nematic phase ($\beta\mu=1.4$).

cal [10,13,29] and simulation [30]. For the cylinder in the nematic phase, the structure of the fluid around the cylinder is highly anisotropic. Two lobes of high order appear at the particle surface, centered around $z \approx \pm 20b$ (above and below the particle with respect to the director far from the particle). There are also two defects (around $x \approx \pm 20b$) to the left and right of the nanoparticle. The director at the particle surface lies parallel to the surface normal, indicating strong radial anchoring. In the isotropic phase (Fig. 2), the structure of the fluid is rotationally invariant, with a layer of orientationally ordered fluid adsorbed on the surface of the cylinder.

Figure 3 shows the structure of a nematic fluid around the nanoparticle near a solid substrate at a number of separations. When the cylinder is far from the wall, the structure around the cylinder is the same as for the isolated cylinder (Fig. 1). The fluid near the substrate shows a distinct layer structure that is undisturbed by the distant cylinder. As the cylinder approaches the substrate, the layer of fluid adsorbed on the surface of the cylinder begins to overlap with the fluid adsorbed on the surface, disturbing the structure of the fluid [Fig. 3(b)]. When the cylinder is closer to the substrate [Fig. 3(c)] the structure is further disturbed, with the defects moving closer to the substrate surface.

The structure around a cylinder near a substrate for the isotropic phase is shown in Fig. 4. As in the nematic phase, when the cylinder is far from the substrate, the structure of the fluid at both the cylinder and the substrate is likewise

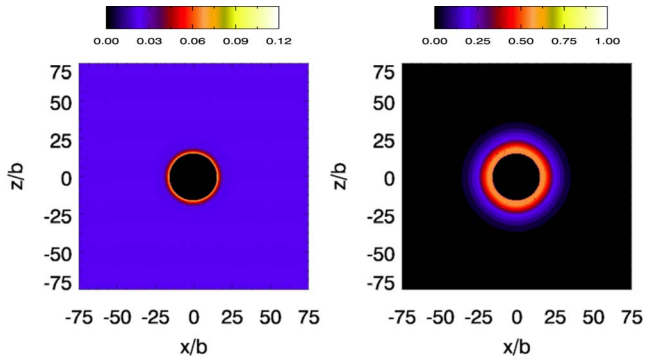

FIG. 2. (Color online) Density (left) and order parameter (right) maps for isolated cylinder in the isotropic phase ($\beta\mu=1.2$).

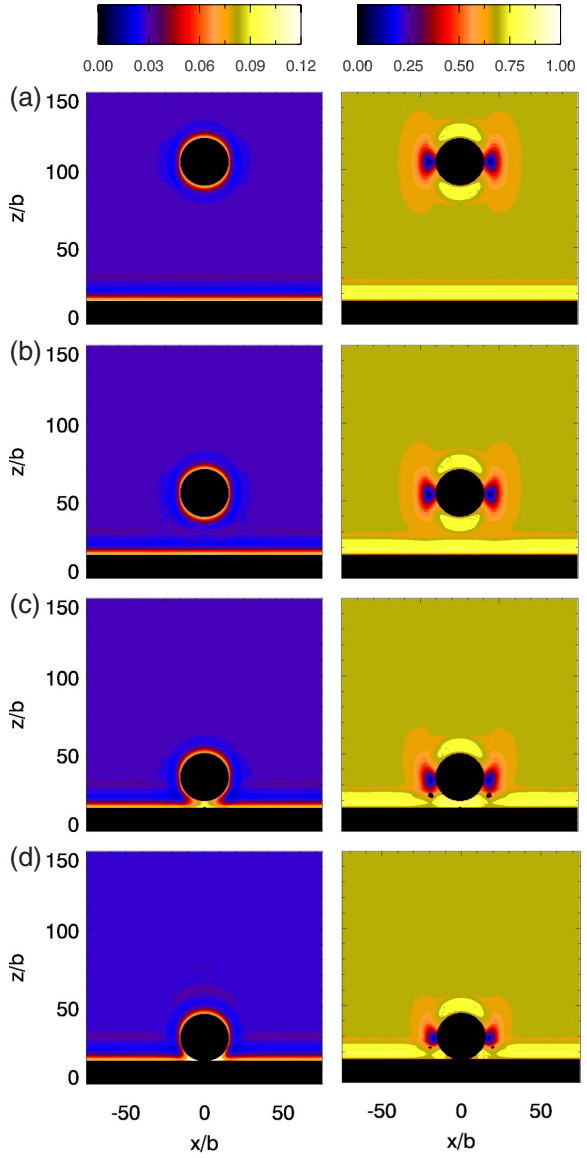

FIG. 3. (Color online) Density (left) and order parameter (right) maps for nanoparticle near substrate with nanoparticle-substrate separation (a) $90b$, (b) $40b$, (c) $20b$, and (d) $15b$ in the nematic phase ($\beta\mu=1.4$).

undisturbed. When the separation between the cylinder and the substrate decreases, a bridge of nematic fluid forms between the substrate and the cylinder. Such capillary bridging has been seen experimentally [15,16] and has been studied for similar systems using phenomenological theories [11]. This gives rise to an attractive interaction between the cylinder and substrate.

The grand potential as a function of z_c (the distance between the nanoparticle centre and substrate) is shown in Fig. 5. There is a marked difference between the variation in the nematic and isotropic phases. In the nematic phase $\Omega(z_c)$ shows little variation with $z_c - R$ beyond $15b$ (one cylinder diameter). There is a significant potential barrier ($3k_BT/L$), that arises due to the overlap between the high-density fluid around the nanoparticle and substrate, and a potential well at

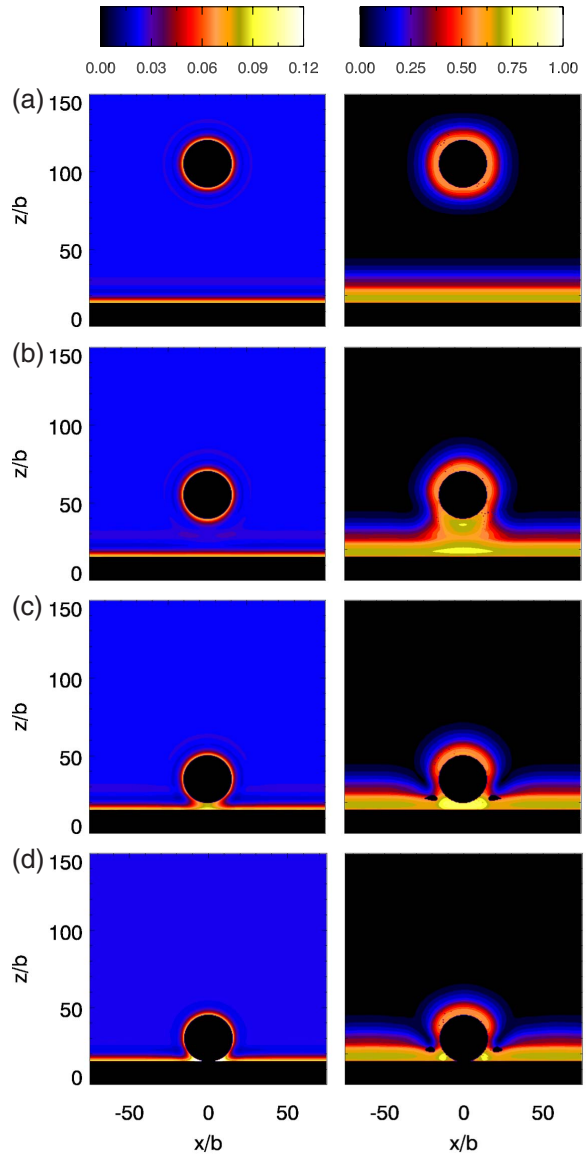

FIG. 4. (Color online) Density (left) and order parameter (right) maps for nanoparticle near substrate with nanoparticle-substrate separation (a) $90b$, (b) $40b$, (c) $20b$, and (d) $15b$ in the isotropic phase ($\beta\mu=1.2$).

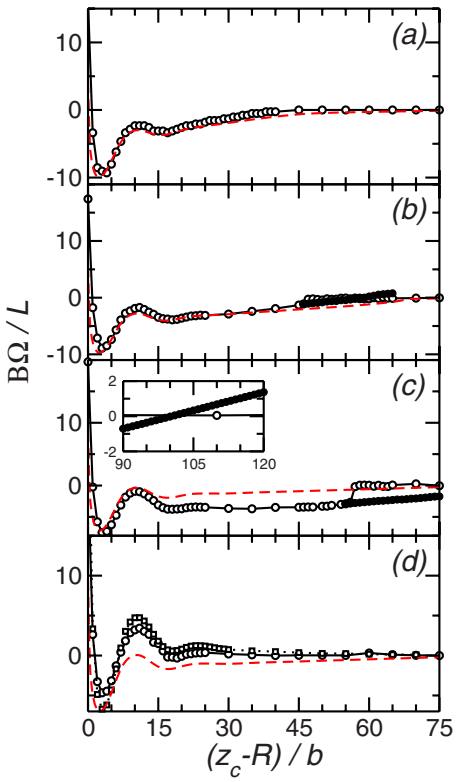

FIG. 5. (Color online) Grand potential (per unit length) as a function of cylinder-substrate separation for solvent chemical potentials $\beta\mu=$(a) 1.0, (b) 1.2, and (c) 1.3 (all isotropic), and (d) $\beta\mu=1.4$ (nematic). Open circles denote Onsager theory results, dashed line shows $\beta\Omega(z_c)/L$ calculated using the Derjaguin approximation. For $\beta\mu=1.2$ and 1.3, $\beta\Omega(z_c)/L$ for the pulled bridged state is shown by the filled circles. Inset in (c) shows the $\Omega(z_c)/L$ for $90b<z_c-R<120b$. For $\beta\mu=1.4$ the squares show $\Omega(z_c)$ for cylinder with $R=30b$.

$z_c-R\approx 3b$ (just over one nanoparticle radius). This is in contrast to Landau–de Gennes (LdG) theory which predicts that at long range $\Omega(z_c)\propto z_c^{-4}$ [9]. To test the effect of increasing cylinder radius $\Omega(z_c)$ has been calculated for cylinder $R=30b$ (Fig. 5). At short range the variation of $\Omega(z_c)$ for this larger radius is similar to that for $R=15b$ with a more pronounced tail. It may be expected that with increasing cylinder radius (with R very much greater than the nematic coherence length) the z_c^{-4} dependence predicted by LdG theory will be found.

When the solvent is in the isotropic phase ($\beta\mu=1.0-1.3$), there is also a potential well at $z_c-R\approx 3b$ and a potential barrier at $z_c-R\approx 10b$. The height of the potential barrier increases and the depth of the well decreases as μ increases. On approaching the isotropic-nematic transition the thickness and density of the adsorbed nematic film on both the cylinder and substrate increase, leading to greater free energy cost when these overlap. By considering $\Omega(z_c)$ for larger separations, the effect of capillary bridging between the nanoparticle and substrate can be clearly seen. The range of this attraction increases as μ increases. At lower chemical potentials, $\Omega(z)$ goes smoothly to zero at large separations. As μ increases the change becomes more abrupt. This abrupt change in energy corresponds to the change between the bridged and nonbridged states. Shown in Fig. 6 are density and order parameter profiles between the substrate and nanoparticle in the solvent isotropic phase for a number of different substrate-nanoparticle separations. For $\beta\mu=1.3$ there is a jump in the order parameter between the substrate and nanoparticle when z_c decreases from $z_c-R=57b$ to $z_c-R=56b$. At $\beta\mu=1.2$ the change occurs slightly more gradually between $z_c-R=47b$ and $z_c-R=45b$. Finally, for $\beta\mu=1.0$ the change is completely smooth with no perceptible jump in $\Omega(z_c)$. Atomic force microscopy measurements of the force between a glass sphere and substrate, in isotropic 5CB and 8CB [15,31], show similar behavior. It should be noted that, on increasing μ from $\beta\mu=1.2$ to $\beta\mu=1.3$, the slope in $\Omega(z_c)$ (hence force) decreases, which differs from

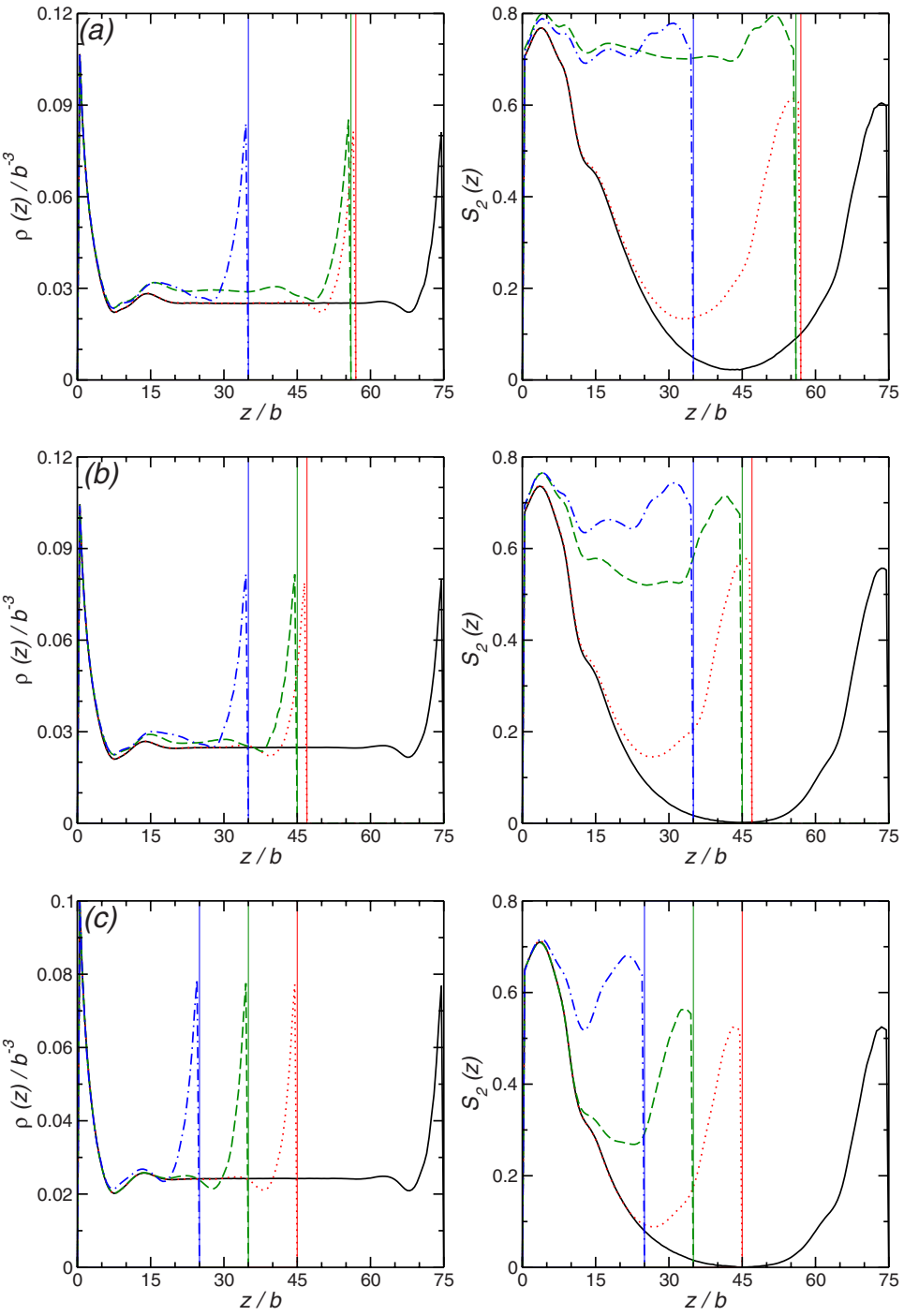

FIG. 6. (Color online) Density (left) and order parameter (right) profiles between substrate and nanoparticle (along the perpendicular from the nanoparticle centre) for solvent chemical potential $\beta\mu$=(a) 1.3, (b) 1.2, and (c) 1.0 for different z_c. Solid line shows $z_c-R=75b$, dotted line (online red) shows $z_c-R=57b$ (a), $47b$ (b), and $45b$ (c), dashed line (online green) shows $z_c-R=56b$ (a), $45b$ (b), and $35b$ (c), and dash-dotted line (online blue) shows $z_c-R=35b$ (a and b) and $25b$ (c). Thin solid lines show position of nanoparticle surface (located at $z=z_c-R$) for different z_c. Note that the abscissa denotes the solvent coordinate z.

the experimental results. The present behavior may be understood as that the change in energy is proportional to the isotropic-nematic interfacial tension (due to changes in the interfacial area between the nematic bridge and isotropic bulk), which will decrease as the isotropic-nematic transition is approached. The experimental forces are also likely to include effects such as fluctuations that are not accounted for in the present approach.

The nature of the transition between the bridged and nonbridged states has been investigated using LdG theory [11]. In agreement with the present results the transition is abrupt for temperatures just above the isotropic-nematic transition

temperature (high μ) and smooth for higher temperatures (low μ). Also in agreement with the present results LdG theory predicts that the separation at which the bridging transition occurs, z_c^b increases as μ increases. Due to the abrupt nature of the bridging transition there is a degree of hysteresis at μ close to the isotropic-nematic transition. By pulling a bridged nanoparticle away from the substrate, $\Omega(z_c)$ for the bridged configurations may be calculated. As may be seen from Fig. 5, $\Omega(z_c)$ shows a linear variation with z_c, which is also related to the increase in interfacial area between the nematic bridge and isotropic bulk. On pulling away from the wall the bridge remains stable for separations beyond z_c^b; for $\beta\mu=1.2$ the bridge persists approximately $(10-15)b$ beyond z_c^b on pulling, while for $\beta\mu=1.3$ it persists for several molecular lengths beyond z_c^b. The inset in Fig. 5(c) shows that $\Omega(z_c)$ for the bridged state remains lower than for the nonbridged state up to $z_c-R\approx 104b$.

The potential between the nanoparticle and substrate may also be calculated using the Derjaguin approximation (DA) [32,33]. This relates the solvent-mediated forces between colloidal particles to the corresponding interactions between parallel planar walls. For the present geometry the potential (per unit length in the y direction) may be written as [34]

$$\frac{\beta\Omega(z_c)}{L}-\frac{\beta\Omega(z_c=\infty)}{L}=\beta\int ds[\gamma(\ell)-2\gamma_\infty],$$

$$\ell=z_c-\sqrt{R_c^2-x^2}, \tag{11}$$

where $\gamma(\ell)$ is the interfacial energy for a planar slit of width ℓ, γ_∞ is the interfacial energy of an isolated planar surface, and $\Omega(z_c=\infty)$ is the grand potential of a nanoparticle at infinite separation from the substrate. $L\,ds$ is an area element of the nanoparticle surface. In terms of the coordinates x and z (where $x^2+z^2=R_c^2$) [34],

$$ds^2=dx^2+dz^2=\frac{R_c^2}{z^2}dx^2. \tag{12}$$

The geometry for this calculation is illustrated in Fig. 7.

As shown in Fig. 5, at low chemical potential $\beta\mu\leqslant 1.2$, Eq. (11) gives reasonable agreement with the numerical results. At low z_c, the DA predicts a repulsive interaction (in agreement with the numerical treatment). By contrast with previous work [35] for rod-shaped molecules, the DA predicts a linear attractive force at small separations. This is likely due to the difference in nanoparticle- and substrate-molecule interactions: in this work these act only on the centers of mass of the fluid molecules, while in Ref. [35] the wall excludes the entire molecule, giving rise to planar alignment at the surface. In the isotropic phase, the DA predicts a longer-range decay of $\Omega(z_c)$ than in the numerical calculations, without an abrupt change at large z_c in the isotropic phase. There is, however, a break in the slope at large z_c: for $\beta\mu=1.2$ this occurs at $z_c-R\approx 68b$, while for $\beta\mu=1.3$ it is at $z_c-R\approx 96b$. This is consistent with capillary condensation between two planar walls, which occurs at separations $\ell=67.5b$ $(\beta\mu=1.2)$ and $\ell=96b$ $(\beta\mu=1.3)$. For all μ, the DA predicts a lower $\Omega(z_c)$ at contact between the wall and nanoparticle. Also, apart from $\beta\mu=1.3$, for all separations, $\Omega(z_c)$ from the DA is lower than in the numerical calculations. This may arise from the neglect of changes in the molecular orientation at the nanoparticle surface in the DA. In the nematic phase, the DA predicts an attractive interaction at large z_c, in contradiction to the numerical results, again due to the neglect of elastic distortions.

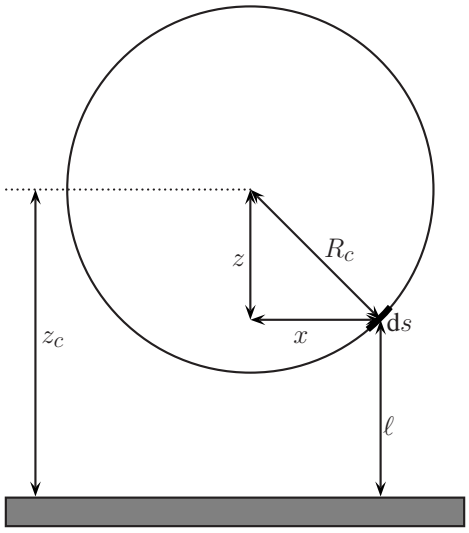

FIG. 7. Geometry for calculation of the depletion interaction using the Derjaguin approximation. R_c is the nanoparticle radius, z_c is the nanoparticle-substrate separation.

IV. CONCLUSIONS

Using DFT, the structure of a molecular fluid around a cylindrical nanoparticle in the vicinity of a solid substrate is studied in both the nematic and isotropic phases. When the cylinder is far from the substrate, the structure of the fluid around both the cylinder and the substrate is undisturbed. As the cylinder approaches the substrate, the structured fluid around them begins to overlap, leading to solvent-mediated interactions between the cylinder and substrate. This interaction is qualitatively different in the nematic and isotropic phases of the solvent.

In the nematic phase this force is largely repulsive and is due to elastic distortions in the LC solvent and overlap between the adsorbed layers of fluid on the cylinder and substrate surfaces. The range of this interaction increases with increasing cylinder radius. In the isotropic phase, an attractive force arises due to the formation of a nematic bridge between the cylinder and substrate. This is similar to the force that causes flocculation of colloidal particles in a LC above the isotropic-nematic (IN) transition. As the IN transition is approached, there is a discontinuous change in the free energy as the separation between the cylinder and substrate decreases. This is caused by the abrupt formation of the nematic bridge, which has been seen experimentally [16] and studied using phenomenological theory [11]. At lower μ the nematic bridge is formed continuously. On increasing

separation there is a smooth variation in the free energy. It may be expected that the strength of the interaction, in both the nematic and isotropic phases, may be varied by changing the anchoring strength on the cylinder and substrate surfaces. Alternatively, the use of a structured substrate may be used to modify the interaction, in particular to give an attractive interaction in the nematic phase [9].

ACKNOWLEDGMENTS

This research was supported by EPSRC Grant No. GR/S77240. The calculations were performed on the computing facilities of the Centre for Scientific Computing, University of Warwick. The authors wish to thank J. R. Henderson for advice regarding the Derjaguin approximation and acknowledge helpful comments from R. Evans and A. Archer.

[1] P. Poulin, Curr. Opin. Colloid Interface Sci. **4**, 66 (1999).
[2] H. Stark, Phys. Rep. **351**, 387 (2001).
[3] W. B. Russel, D. A. Saville, and W. R. Schowalter, *Colloidal Dispersions* (Cambridge University Press, Cambridge, U.K., 1989).
[4] T. Hegmann, H. Qi, and V. M. Marx, J. Inorg. Organomet. Polym. **17**, 483 (2007).
[5] J. S. van Duijneveldt, S. Klein, E. Leach, C. Pizzey, and R. M. Richardson, J. Phys.: Condens. Matter **17**, 2255 (2005).
[6] C. Lapointe, A. Hultgren, D. M. Silevitch, E. J. Felton, D. H. Reich, and R. L. Leheny, Science **303**, 652 (2004).
[7] V. K. Gupta, J. J. Skaife, T. B. Dubrovsky, and N. L. Abbot, Science **279**, 2077 (1998).
[8] M. Lynch and D. Patrick, Nano Lett. **2**, 1197 (2002).
[9] N. M. Silvestre, P. Patricio, and M. M. Telo da Gama, Phys. Rev. E **69**, 061402 (2004).
[10] D. Andrienko, M. Tasinkevych, P. Patrício, and M. M. Telo da Gama, Phys. Rev. E **69**, 021706 (2004).
[11] H. Stark, J. I. Fukuda, and H. Yokoyama, Phys. Rev. Lett. **92**, 205502 (2004).
[12] D. Andrienko, G. Germano, and M. P. Allen, Phys. Rev. E **63**, 041701 (2001).
[13] D. L. Cheung and M. P. Allen, Phys. Rev. E **74**, 021701 (2006).
[14] L. Onsager, Ann. N.Y. Acad. Sci. **51**, 627 (1949).
[15] K. Kočevar and I. Muševič, Phys. Rev. E **64**, 051711 (2001).
[16] K. Kočevar and I. Muševič, ChemPhysChem **4**, 1049 (2003).
[17] A. R. Herring and J. R. Henderson, Phys. Rev. Lett. **97**, 148302 (2006).
[18] A. R. Herring and J. R. Henderson, Phys. Rev. E **75**, 011402 (2007).
[19] M. P. Allen, G. T. Evans, D. Frenkel, and B. Mulder, Adv. Chem. Phys. **86**, 1 (1993).
[20] J.-P. Hansen and I. R. McDonald, *Theory of Simple Liquids*, 2nd ed. (Academic Press, London, 1986).
[21] P. J. Camp, C. P. Mason, M. P. Allen, A. A. Khare, and D. A. Kofke, J. Chem. Phys. **105**, 2837 (1996).
[22] S. V. Burylov and Y. L. Raikher, Phys. Rev. E **50**, 358 (1994).
[23] J. J. Skaife, J. M. Brake, and N. L. Abbott, Langmuir **17**, 5448 (2001).
[24] D. Andrienko and M. P. Allen, Phys. Rev. E **65**, 021704 (2002).
[25] C. G. Gray and K. E. Gubbins, *Theory of Molecular Fluids. 1. Fundamentals* (Clarendon Press, Oxford, 1984).
[26] W. H. Press, B. P. Flannery, S. A. Teukolsky, and W. T. Vetterling, *Numerical Recipes* (Cambridge University Press, Cambridge, U.K., 1986).
[27] V. I. Lebedev, Zh. Vychisl. Mat. Mat. Fiz. **16**, 293 (1976) [USSR Comput. Math. Math. Phys. **16** 10 (1976)].
[28] V. I. Lebedev, Sib. Math. J. **18**, 99 (1977).
[29] R. Yamamoto, Y. Nakayama, and K. Kim, J. Phys.: Condens. Matter **16**, S1945 (2004).
[30] D. Andrienko, M. P. Allen, G. Skačej, and S. Žumer, Phys. Rev. E **65**, 041702 (2002).
[31] A. Borštnik Bračič, K. Kočevar, I. Muševič, and S. Žumer, Phys. Rev. E **68**, 011708 (2003).
[32] J. N. Israelachvili, *Intermolecular and Surface Forces*, 2nd ed. (Academic, London, 1992).
[33] B. V. Derjaguin, Kolloid-Z. **69**, 155 (1934).
[34] J. R. Henderson, Physica A **313**, 321 (2002).
[35] Y. Mao, M. E. Cates, and H. N. W. Lekkerkerker, J. Chem. Phys. **106**, 3721 (1997).